

# The 2XMMi/SDSS Galaxy Cluster Survey

## III. Clusters associated with spectroscopically targeted luminous red galaxies in SDSS-DR10

A. Takey<sup>1,2</sup>, A. Schwoppe<sup>1</sup>, and G. Lamer<sup>1</sup>

<sup>1</sup> Leibniz-Institut für Astrophysik Potsdam (AIP), An der Sternwarte 16, 14482 Potsdam, Germany  
e-mail: atakey@aip.de

<sup>2</sup> National Research Institute of Astronomy and Geophysics (NRIAG), 11421 Helwan, Cairo, Egypt

Received ....; accepted ....

### ABSTRACT

We present a sample of 383 X-ray selected galaxy groups and clusters with spectroscopic redshift measurements (up to  $z \sim 0.79$ ) from the 2XMMi/SDSS Galaxy Cluster Survey. The X-ray cluster candidates were selected as serendipitously detected sources from the 2XMMi-DR3 catalogue that were located in the footprint of the Sloan Digital Sky Survey (SDSS-DR7). The cluster galaxies with available spectroscopic redshifts were selected from the SDSS-DR10. We developed an algorithm for identifying the cluster candidates that are associated with spectroscopically targeted luminous red galaxies and for constraining the cluster spectroscopic redshift. A cross-correlation of the constructed cluster sample with published optically selected cluster catalogues yielded 264 systems with available redshifts. The present redshift measurements are consistent with the published values. The current cluster sample extends the optically confirmed cluster sample from our cluster survey by 67 objects. Moreover, it provides spectroscopic confirmation for 78 clusters among our published cluster sample, which previously had only photometric redshifts. Of the new cluster sample that comprises 67 systems, 55 objects are newly X-ray discovered clusters and 52 systems are sources newly discovered as galaxy clusters in optical and X-ray wavelengths. Based on the measured redshifts and the fluxes given in the 2XMMi-DR3 catalogue, we estimated the X-ray luminosities and masses of the cluster sample.

**Key words.** X-rays: galaxies: clusters, galaxies: clusters: general, surveys, catalogs, techniques: spectroscopic

### 1. Introduction

Galaxy clusters are the largest gravitationally bound objects in the Universe. They have been formed from the densest regions in the large-scale matter distribution of the Universe and have collapsed to form their own proper equilibrium structure. Their form can be well assessed by observations and well described by theoretical modelling (e.g. Sarazin 1988; Bahcall 1988; Voit 2005; Böhringer 2006; Ota 2012). X-ray and optical observations show that galaxy clusters are clearly defined connected structural entities, where the diffuse X-ray emission from the hot intracluster medium (ICM) trace the whole structure of the cluster. They are excellent giant laboratory sites for several astrophysical studies, for example, investigating galaxy evolution in their dense environments (e.g. Dressler 1980; Goto et al. 2003), evolution of the dynamical and thermal structure (e.g. Balestra et al. 2007; Maughan et al. 2008; Anderson et al. 2009), chemical enrichment of the intracluster medium (e.g. Cora 2006; Heath et al. 2007), studying lensed high-redshift background galaxies (e.g. Metcalfe et al. 2003; Santos et al. 2004; Bartelmann 2010), and investigating the evolution of the Universe to test the cosmological models (e.g. Rosati et al. 2002; Reiprich & Böhringer 2002; Voit 2005; Vikhlinin et al. 2009; Allen et al. 2011).

Owing to the multi-component nature of galaxy clusters, they can be observed and identified through multiple observable signals across the electromagnetic spectrum. Tens of thousands of galaxy clusters have been identified by detecting their galaxies in the optical and near-infrared (NIR) bands (e.g. Abell 1958;

Abell et al. 1989; Zwicky et al. 1961; Gladders & Yee 2005; Merchán & Zandivarez 2005; Koester et al. 2007; Wen et al. 2009; Hao et al. 2010; Szabo et al. 2011; Geach et al. 2011; Durret et al. 2011; Wen et al. 2012; Gettings et al. 2012; Rykoff et al. 2013). Recently, several galaxy cluster surveys have been conducted at mm wavelengths using the Sunyaev-Zeldovich (SZ) effect based on observations made by several instruments, for example, the Atacama Cosmology Telescope (ACT, Hasselfield et al. 2013), the South Pole Telescope (SPT, Reichardt et al. 2013), and the Planck Satellite (Planck Collaboration et al. 2013). These surveys have provided cluster samples that contain several hundreds of SZ-selected clusters.

X-ray cluster surveys provide pure and complete cluster catalogues, in addition, their X-ray observables correlate tightly with masses of clusters (e.g. Allen et al. 2011). Several hundreds of galaxy clusters were detected in X-rays based on previous X-ray missions mainly from ROSAT data (e.g. Ebeling et al. 1998; Böhringer et al. 2004; Reiprich & Böhringer 2002; Ebeling et al. 2010; Rosati et al. 1998; Burenin et al. 2007). The current X-ray telescopes (XMM-Newton, Chandra, Swift/X-ray) provide contiguous cluster surveys for small areas (e.g. Finoguenov et al. 2007, 2010; Adami et al. 2011; Šuhada et al. 2012), in addition to serendipitous cluster surveys (e.g. Barkhouse et al. 2006; Kolokotronis et al. 2006; Lamer et al. 2008; Fassbender et al. 2011; Takey et al. 2011; Mehrrens et al. 2012; Clerc et al. 2012; Tundo et al. 2012; de Hoon et al. 2013; Takey et al. 2013). So

far, these surveys have provided a substantial cluster sample of several hundreds up to a redshift of 1.57.

We have conducted a systematic search for X-ray detected galaxy clusters based on XMM-Newton fields that are located in the footprint of the SDSS-DR7. The catalogue of serendipitously detected sources (extended) in XMM-Newton EPIC images was the basic database from which we selected a list of X-ray cluster candidates, comprising 1180 objects. The main goal of the survey is to construct a large catalogue of newly discovered X-ray emitting groups and clusters. Due to the higher sensitivity of XMM-Newton the compiled cluster sample extends ROSAT cluster samples to fainter X-ray fluxes. The sample, which comprised galaxy groups and clusters, allows us to investigate the evolution of X-ray scaling relations as well as the correlation between the X-ray and optical properties. Other long-term goals of the survey are the selection of distant clusters beyond the SDSS detection limit and, in general terms, the preparation for the eROSITA mission, which will uncover a similar cluster population as in our survey.

The main way to obtain the cluster redshifts is based on the optical data. This can be achieved by either cross-matching the X-ray cluster candidates with the available optically selected galaxy cluster catalogues in the literature or by measuring the cluster photometric redshifts based on galaxy redshifts given in the SDSS catalogues. Using these two methods, we were able to establish an optically confirmed cluster sample comprising 530 groups/clusters with redshift measurements. From these optically confirmed groups/clusters with redshift measurements, we derived their X-ray luminosities and temperatures and investigated the X-ray luminosity-temperature relation. The selection criteria of the X-ray cluster candidates and redshift measurements as well as the X-ray properties of the optically confirmed sample were described in more detail by Takey et al. (2011, 2013, Paper I, Paper II, hereafter).

In this work, we compile a sample of X-ray detected galaxy clusters among the X-ray cluster candidate list that are associated with luminous red galaxies (LRGs), which have spectroscopic redshift measurements out to 0.8 in the SDSS-DR10. We present the procedure we used for constructing this cluster sample that is spectroscopically confirmed and for measuring their redshifts. We also present estimates of X-ray bolometric luminosity and luminosity-based mass at  $R_{500}$  (the radius at which the cluster mean density is 500 times the critical density of the Universe at the cluster redshift) of the cluster sample.

The compiled cluster sample can be used to investigate various relations among the cluster physical properties, for example, the correlations between the properties of the BCG and its hosting cluster. By measuring the X-ray temperature of the cluster sample, one can extend the  $L_X - T$  relation in Paper II to slightly higher redshifts. Moreover, the cluster sample is expected to permit studies of the relations between the cluster optical properties (richness and luminosity) and the cluster X-ray properties (X-ray temperature, luminosity, and mass). These correlations will be discussed in an upcoming paper.

The article is organized as follows: Section 2 gives a short overview on the selection procedure of the X-ray cluster candidates. In Section 3, we describe the construction of the cluster sample associated with LRGs and their redshift measurements. The X-ray parameters of the cluster sample are presented in Section 4. The summary of the paper is presented in Section 5. Throughout this paper, we used the cosmological parameters  $\Omega_M = 0.3$ ,  $\Omega_\Lambda = 0.7$  and  $H_0 = 70 \text{ km s}^{-1} \text{ Mpc}^{-1}$ .

## 2. Description of the X-ray cluster candidates

Galaxy clusters are simply identified among the X-ray sources as X-ray luminous, spatially extended, extragalactic sources (Allen et al. 2011). The largest X-ray source catalogue so far is the XMM-Newton serendipitous source catalogue, which has been created by the XMM-Newton Survey Science Centre (SSC). The latest edition of this catalogue is the 3XMM-DR4<sup>1</sup>, which contains 372728 unique X-ray sources drawn from 7427 XMM-Newton EPIC observations made between 2000 February 3 and 2012 December 8. Our survey was based on the previous edition of the XMM-Newton serendipitous source catalogue (2XMMi-DR3<sup>2</sup>, Watson et al. 2009) that was compiled based on 4953 XMM-Newton observations made between 2000 February 3 and 2009 October 8. The 2XMMi-DR3 catalogue comprises 353191 detections corresponding to 262902 unique sources. Of these detections, 30470 are extended detections, which include both real and spurious extended sources as well as multiple detections of the same sources.

We selected the X-ray cluster candidates from reliable extended sources (with no warning about being spurious) in the 2XMMi-DR3 catalogue at high galactic latitudes,  $|b| > 20^\circ$ . The survey was constrained to the XMM-Newton fields that were located in the footprint of the SDSS-DR7 to be able to measure the optical redshifts of the possible optical counterparts. The overlap area of XMM-Newton fields and the imaging area of the SDSS-DR7 is  $210 \text{ deg}^2$ . After excluding possible spurious X-ray extended detections and low-redshift galaxies that appear resolved at X-ray wavelengths through visual inspections of the X-ray images and the X-ray-optical overlays, the X-ray cluster candidate list comprised 1180 objects. The selection procedure was described in more detail in papers I and II.

In this paper, we identify a subsample of these X-ray cluster candidates associated with LRGs that have spectroscopic redshifts in the SDSS-DR10 to construct a sample with spectroscopic confirmations. As an example, Fig. 1 shows a galaxy cluster, 2XMMi J143742.9+340810, at a redshift of 0.5446, associated with two LRGs as cluster member galaxies with available spectroscopic redshifts. We use this cluster to show the procedure of measuring the redshift in the next section.

## 3. Clusters associated with spectroscopically targeted LRGs in SDSS-DR10

Generally, the brightest cluster galaxies (BCGs) are elliptical massive galaxies and reside near the cluster centre of mass. The BCGs tend to be very luminous and red galaxies (e.g. Postman & Lauer 1995; Eisenstein et al. 2001; Wen et al. 2012), therefore they have a good chance to be selected for BOSS spectroscopy in SDSS-III as members of the LRG sample, which in turn allows a straightforward spectroscopic confirmation of associated galaxy clusters (e.g. Goto et al. 2002; Mehtens et al. 2012).

We identified the LRGs from the SDSS-DR10 data that are cluster member galaxies of the X-ray cluster candidates. The spectroscopic redshifts of these cluster members were used to measure the cluster redshift. In the next subsections, we describe how we selected the LRGs from the recent data of the SDSS and the procedure we followed to measure the cluster redshift. We also present some statistical properties of the constructed cluster sample, such as the redshift distribution and the projected offsets

<sup>1</sup> [http://xmmssc-www.star.le.ac.uk/Catalogue/xcat\\_public\\_3XMM](http://xmmssc-www.star.le.ac.uk/Catalogue/xcat_public_3XMM)

<sup>2</sup> [http://xmmssc-www.star.le.ac.uk/Catalogue/xcat\\_public\\_2XMM](http://xmmssc-www.star.le.ac.uk/Catalogue/xcat_public_2XMM)

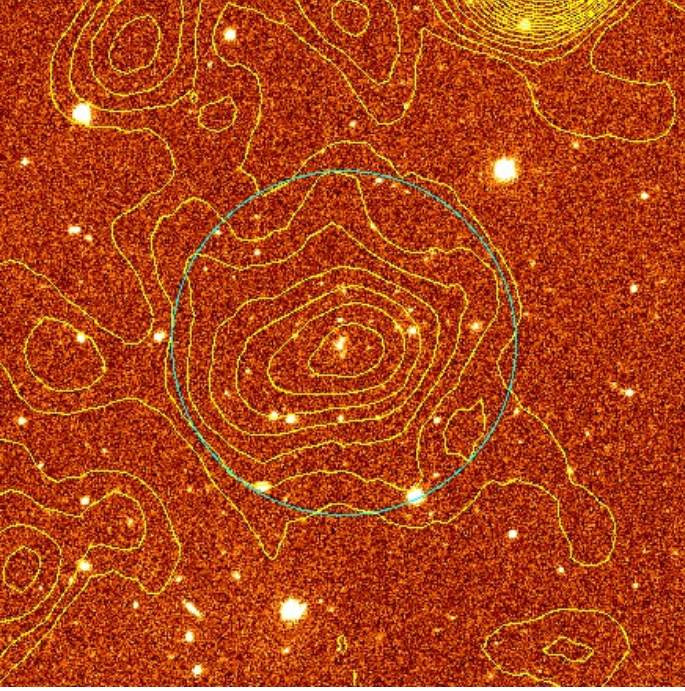


**Fig. 1.** SDSS image of the cluster 2XMMi J143742.9+340810 at a redshift of 0.5446, with X-ray surface brightness contours (0.2 - 4.5 keV) overlaid in yellow. The plotted cyan circle has a radius of one arcmin around the X-ray position. The field of view is  $4' \times 4'$  centred on the X-ray emission peak.

of the BCGs from the X-ray positions. Then a comparison of the current redshift measurements with the published ones is presented. Finally, we give a general overview of the total optically confirmed cluster sample from our survey.

### 3.1. Luminous red galaxy sample

The Sloan Digital Sky Survey (SDSS) has been in continuous operation since 2000. The latest data release so far from the SDSS is Data Release 10 (SDSS-DR10, Ahn et al. 2013), which provides the spectroscopic data from the SDSS-III's Baryon Oscillation Spectroscopic Survey (BOSS) as well as imaging and spectroscopic data from the previous SDSS data releases. SDSS-DR10 provides optical spectra for 1880584 galaxies. BOSS is an ongoing project and its current data release includes 927844 galaxy spectra, in addition to thousands of quasar and stellar spectra, which were selected over  $6373.2 \text{ deg}^2$ . One aim of BOSS is to obtain spectra of 1.5 million galaxies in the redshift range of  $0.15 < z < 0.8$  distributed over  $10000 \text{ deg}^2$ . Therefore, it is a valuable resource to obtain spectroscopic redshifts for luminous cluster galaxies.

Luminous red galaxies are among the most luminous red galaxies that can be observed up to redshift 0.8 with SDSS equipment. As a starting point for identifying LRGs that are expected to be cluster galaxies, we selected all galaxies within 10 arcmin of the X-ray position, which is the maximum angular scale at the low-redshift end (500 kpc at  $z = 0.04$ ) to be considered for our cluster candidate sample. In a second iteration step, we refined this search radius according to the initial cluster redshift estimate based on the redshift of the BCG candidate. The galaxies were selected from the galaxy view table in the SDSS-DR10, which contains the photometric parameters measured for resolved primary objects, classified as galaxies.

The photometric redshifts ( $z_p$ ) and, where available, the spectroscopic redshifts ( $z_s$ ) of the galaxy sample were also selected from the Photoz and SpecObj tables, respectively. The SpecObj table includes spectroscopic redshifts that were measured from clean galaxy spectra taken by the new and old spectrographs in the SDSS projects. The extracted parameters of the galaxy sample included the coordinates, the (model and composite model) magnitudes in  $r$ - and  $i$ -bands, the photometric redshifts, and, where available, the spectroscopic redshifts. We used the magnitudes in the galaxy table that are corrected for Galactic extinction following Schlegel et al. (1998). To clean the galaxy sample from faint objects beyond the completeness limits of SDSS or from galaxies with large uncertainty in  $z_p$ , we only considered galaxies that have a model magnitude of  $m_r \leq 22.2$  mag and  $\Delta m_r < 0.5$  mag and a relative error of photometric redshift of  $\Delta z_p / z_p < 0.5$ .

The BOSS data include two main target galaxy samples; first the BOSS LOWZ galaxy sample with  $z \leq 0.4$ ; second the BOSS constant-mass CMASS galaxy sample with  $0.4 < z < 0.8$ . The target selection algorithms for galaxies in BOSS are significantly different from those used in the previous SDSS projects because of the different scientific goals (Ahn et al. 2012). BOSS galaxy targets are significantly fainter than those in the previous SDSS projects with the aim of measuring large-scale clustering of galaxies at higher redshifts.

To select a homogeneous luminous red galaxy sample from BOSS and previous SDSS data releases, we applied the same selection criteria on both data. We selected LRGs with available spectroscopic redshifts from the constructed galaxy sample within 10 arcmin from the X-ray positions. The applied selection criteria of LRGs were based on the colour and magnitude cuts that are described by Padmanabhan et al. (2014, in preparation) and given on the SDSS website<sup>3</sup> as well as in Appendix A. We also ensured that the selected objects are confirmed galaxies using the spectroscopic class parameter given in the SpecObj table to exclude objects targeted as galaxies that were stars or quasars. The selected LRG sample was used to identify the BCGs of the X-ray cluster candidates as described in the following subsection.

### 3.2. Optical identifications and redshift measurements

To measure the redshifts of cluster candidates, we firstly identified the BCG candidates, then we selected cluster member candidates with available similar  $z_s$  of the BCG's spectroscopic redshift. The procedure works as follows:

1. We identified a BCG candidate as an LRG within 200 kpc (computed based on  $z_s$  of the LRG) from the X-ray position of the cluster candidate. If there was only one LRG, we considered it as the BCG candidate. If there were several LRGs, we divided them into groups with similar redshifts that are within a redshift interval of  $\Delta z_s = 0.01$ . When there was only one group, we chose the brightest LRG as the BCG candidate. If there was more than one group, the priority was given to the group with more members and the BCG candidate was selected as the brightest galaxy from this group. If the groups have the same count of LRGs, we initially selected the brightest galaxy in each group. Then the next-brightest LRG to the X-ray emission peak was regarded as the BCG candidate. The maximum number of LRGs within 200 kpc from the X-ray centre was four.

<sup>3</sup> [http://www.sdss3.org/dr10/algorithms/boss\\_galaxy\\_ts.php](http://www.sdss3.org/dr10/algorithms/boss_galaxy_ts.php)

At low redshifts, the search radius of 200 kpc subtends a large angle on the sky and might cause an incorrect association of LRGs with the X-ray cluster candidates. Therefore, we set a maximum angular separation limit on the BCGs offset from the X-ray emission peak of 90 arcsec. The search radius of 200 kpc was used since we found that 90 percent of the BCGs in Paper II had an offset lower than 200 kpc. The search radius (200 kpc) used here is slightly larger than the search radius (175 kpc) used by Mehrtens et al. (2012) to identify LRGs that are part of the cluster. These authors assigned the spectroscopic redshift of an LRG or a group of LRGs within 175 kpc from the X-ray position as the cluster redshift.

2. We identified the cluster member candidates (not necessarily LRGs) within 500 kpc from the X-ray peak based on the spectroscopic redshift of the identified BCG candidate,  $z_{s,BCG}$ . The cluster galaxies with available  $z_s$  were selected within a small redshift interval of  $z_{s,BCG} \pm 0.01$ . While the cluster member candidates with only  $z_p$  were selected within a slightly larger redshift interval of  $z_{s,BCG} \pm 0.04(1 + z_{s,BCG})$ . The distribution of the redshifts of the cluster member candidates and field galaxies for the example cluster is shown in Fig. 2. The redshift interval we used to identify the cluster members with  $z_p$  gives 80 percent of the cluster members (Wen et al. 2009). These authors also showed that a radius of 500 kpc gives a high overdensity level and a low false-detection rate. The identified BCG candidate could be a cluster galaxy fainter than the first BCG, thus we re-identified the likely BCG as the brightest galaxy among the cluster member candidates within 500 kpc.
3. We computed the spectroscopic,  $\bar{z}_s$ , and photometric,  $\bar{z}_p$ , redshift of a cluster as a weighted average of the spectroscopic and photometric redshifts of the cluster member candidates within 500 kpc, respectively. The weights are given as  $w_i = 1/(\Delta z_{s,i})^2$  in computing  $\bar{z}_s$  and as  $w_i = 1/(\Delta z_{p,i})^2$  in determining  $\bar{z}_p$ . If there was only one cluster galaxy (LRG) with available spectroscopic redshift  $z_s$ , we considered its  $z_s$  as the cluster redshift.
4. We accepted the optical counterpart and the redshift measurement of an X-ray cluster candidate if the optical detection passed the quality assessment performed through a visual inspection process. We compared the identified BCG and cluster member candidates with the corresponding SDSS colour image of the same field. The sky distribution of cluster members of the example cluster is shown in Fig. 3, while Fig. 4 shows the corresponding SDSS colour image. From both images, it was obvious that the algorithm picked the correct associated LRGs (and thus the BCG too) and the luminous cluster member candidates. The fainter cluster galaxies were not considered in Fig. 3 because of the magnitude limit we used to create the galaxy sample or they were not detected at all in Fig. 4 because of the detection limit of the SDSS imaging.

The current procedure yielded an initial list of optical counterparts that comprised 415 candidates. We regard about 8 percent of the initial candidates as doubtful for two main reasons, overlapping clusters and unrelated nearby galaxies. We found cases of most likely overlapping clusters where the algorithm probably picked an incorrect cluster since an LRG of this not-so-distant cluster happened to lie closer to the X-ray position. Another reason for an incorrect redshift estimate is the identification of a bright foreground galaxy as BCG candidate for a distant cluster candidate, where no detected cluster galaxies are

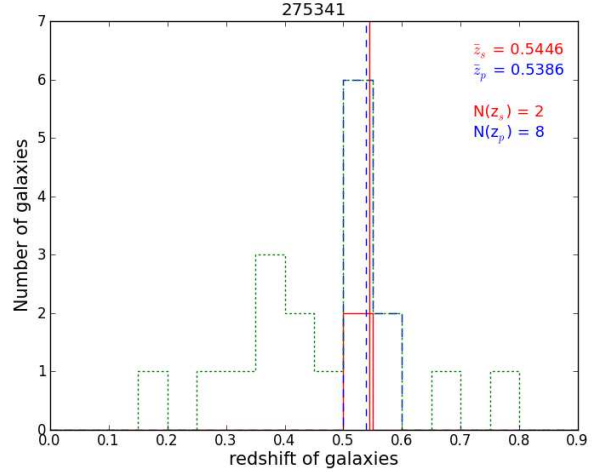


**Fig. 2.** Histogram of the spectroscopic ( $z_s$ , red solid) and photometric ( $z_p$ , blue dashed) redshifts of the cluster member candidates ( $N_{z_s}$  and  $N_{z_p}$ ) within 500 kpc of the example cluster, 2XMMi J143742.9+340810. The green dotted histogram represents the distribution of  $z_p$  of field galaxies within the same region. The cluster spectroscopic  $\bar{z}_s$  and photometric  $\bar{z}_p$  redshifts are represented by red solid and blue dashed vertical lines, respectively, and are listed in the upper corner.

found around the X-ray emission peak. We excluded such systems from the initial cluster candidate sample. Therefore, the estimated misidentification fraction of the resulting optical counterpart list using the current cluster identification procedure is about 8 percent. These systems were removed from the sample without additional attempts to correct for or quantify their effect. The final list of the optically validated cluster sample included 383 systems with spectroscopic confirmation based on at least one spectrum of an LRG.

### 3.3. Optically validated cluster sample

The redshifts of the optically confirmed cluster sample (383 systems) span a wide range from 0.05 to 0.79 with a median of 0.34. Among this sample, 147 clusters are spectroscopically confirmed based only on the SDSS-III BOSS data. The redshift distribution of the current cluster sample (383 systems), the subsample based only on BOSS survey (147 objects), and the optically confirmed cluster sample (530 systems) in Paper II are shown in Fig. 5. The redshift distribution of the current cluster sample is dependent on the selection of LRG targets in SDSS projects and the selection of X-ray cluster candidates from the 2XMMi-DR3 catalogue as well as the cluster identification procedure we used here to construct the cluster sample. The drop of the redshift histogram at  $z = 0.60 - 0.65$  might be a result of a combination of these effects or possibly the low-statistics regime of the survey.

The objects in common between the two samples (Paper II sample and the current one) are 316 systems, see the next subsection for the redshift comparison. The current cluster sample includes 40 more distant clusters beyond  $z = 0.5$  than the distant sample in Paper II. As shown in Fig. 5, these distant clusters were detected based on BOSS data, thanks to the data release of BOSS in the SDSS-DR10. Additionally, the current cluster sample extends the confirmed cluster sample in Paper II by 67 systems, of these 52 systems are newly discovered galaxy clus-

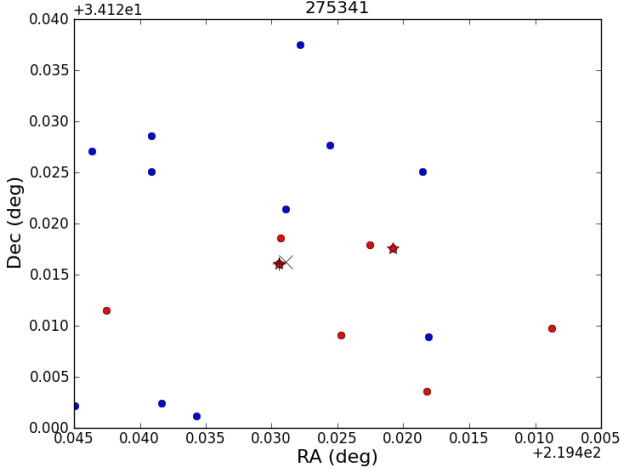


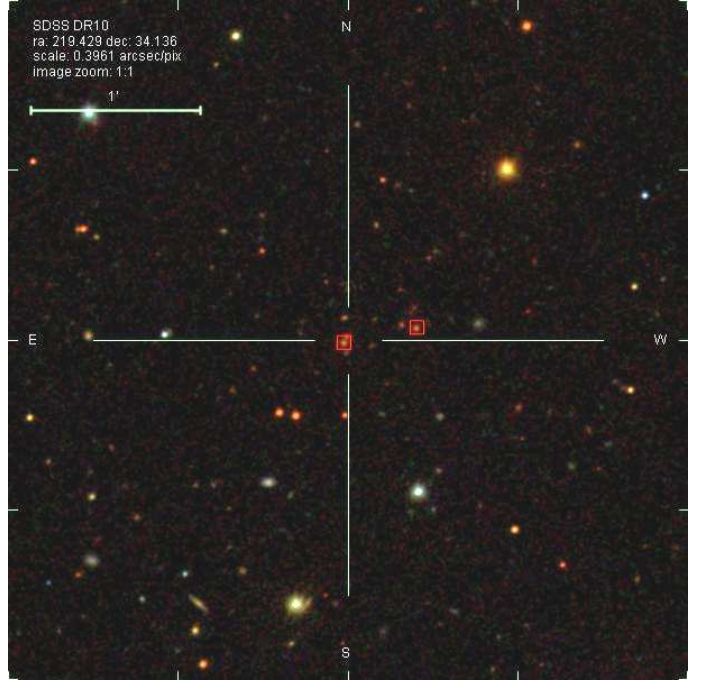
**Fig. 3.** Distribution on the sky of the cluster member candidates (red dots) and field galaxies (blue dots) within 500 kpc ( $\sim 1.3$  arcmin) from the X-ray position (marked by a black cross) of the example cluster, 2XMMi J143742.9+340810. Note the different scale in Fig. 4. The cluster galaxies with available  $z_s$  are marked by stars. The BCG candidate is marked by a black plus that has a projected separation from the X-ray position of  $\sim 11$  kpc. We only present galaxies with  $m_r \leq 22.2$  mag,  $\Delta m_r < 0.5$  mag, and  $\Delta z_p/z_p < 0.5$ .

ters. Therefore, the current cluster sample is complementary to that presented in Paper II in terms of size and redshift range. Both samples can be combined for future investigations of X-ray scaling relations as well as X-ray-to-optical relations.

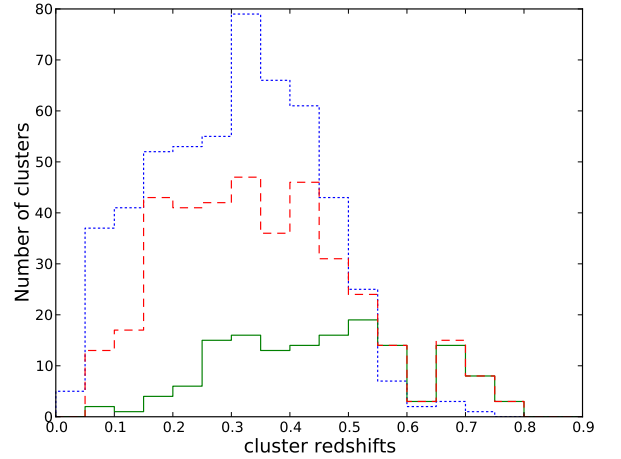
The majority of the clusters in the sample have one or two cluster member galaxies with  $z_s$ , while few clusters have three member galaxies or more with available  $z_s$ . The distribution of the cluster galaxies with  $z_s$  per cluster of the cluster sample is shown in Fig. 6. The cluster member galaxies are not complete for the distant systems in our cluster sample. Faint cluster galaxies were not considered or detected because of the magnitude limit (SDSS completeness limit) used in the current procedure or the limited data depth of the SDSS imaging, respectively. For instance, only the BCG (LRG) was identified for the most distant cluster in the sample at a redshift of 0.79.

Figure 7 shows the scatter plot between the count of identified cluster member candidates per system with  $z_p$  and within 500 kpc from the X-ray position and the cluster redshift. It is shown that distant clusters have only a few identified luminous cluster galaxies, mainly because of the sensitivity limits of the SDSS. We kept these objects in our cluster candidate list, even with only two member galaxies, for the summed evidence of extended X-ray emission positioning that coincides with an LRG with spectra. To determine a complete cluster richness, one needs to follow-up these systems to obtain deep imaging data.

Based on the cluster redshift and the angular separation of the BCGs to the X-ray peaks, we computed their projected offsets. The distribution of the projected separations between the probable BCGs and the X-ray emission peaks is shown in Fig. 8. We found that the majority of the BCGs (about 90 percent) have offsets smaller than 200 kpc, which agree with the offsets of BCGs sample in Paper II. By using the current selection procedure of the BCG as a cluster member galaxy within 500 kpc from the X-ray centers, the maximum offset is about 500 kpc. The large offset of the BCGs from the X-ray centroids might ap-



**Fig. 4.** SDSS colour image of the cluster 2XMMi J143742.9+340810 with 4 arcmin a side centered on the X-ray position, which is marked by the cross-hair. Two cluster galaxies (LRGs) with spectra are marked by red squares. The measured spectroscopic redshift for this system is 0.5446, which is computed as the weighted average,  $\bar{z}_s$ , of the spectroscopic redshifts of the two LRGs.



**Fig. 5.** Distribution of measured spectroscopic redshifts of the cluster sample associated with LRGs that have spectra is presented by the red dashed line, and a subsample of it based only on BOSS data is indicated by the green solid line, while the redshift distribution of the optically confirmed cluster sample in Paper II is presented by the blue dotted line.

pear in systems with an ongoing merger or in dynamically active clusters (Rykoff et al. 2008).

The distribution of positional offsets of the BCGs from the X-ray positions might be biased by the initial LRG (BCG candidate) selection, which was required to lie within a projected distance of 200 kpc. Since we excluded apparent doubtful systems

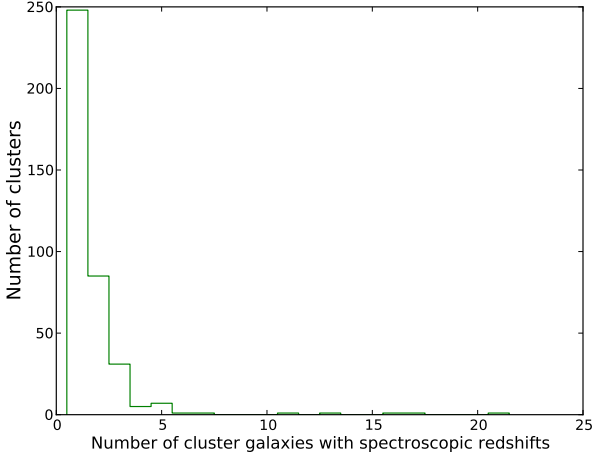


**Fig. 6.** Distribution of the number of identified spectroscopic cluster galaxies per system within 500 kpc from the X-ray positions for the optically validated cluster sample. The bin size of the histogram is one.

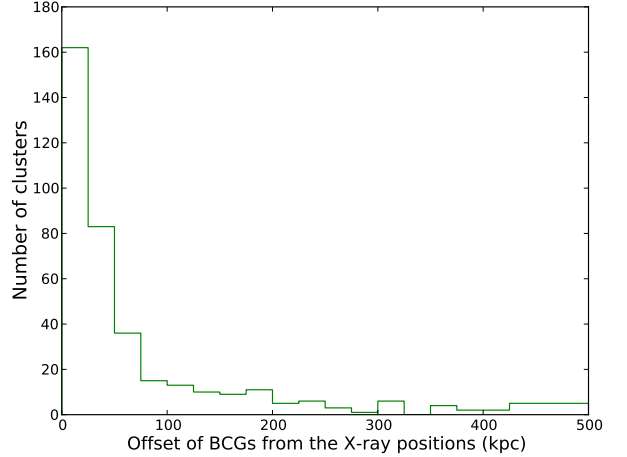


**Fig. 8.** Histogram of the projected separations between the probable BCGs and the X-ray emission peaks of the cluster sample.

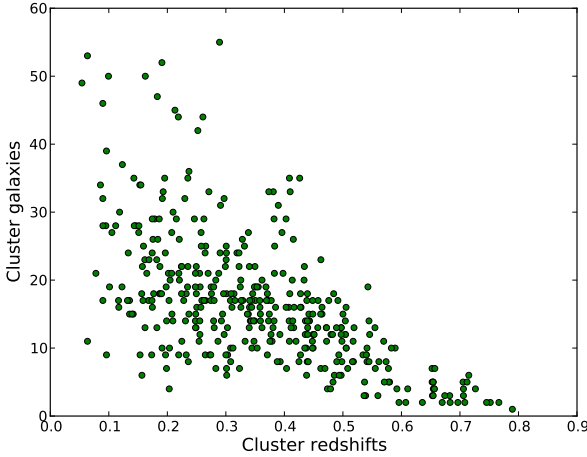


**Fig. 7.** Cluster member galaxies plotted against the cluster spectroscopic redshifts. These cluster member candidates were selected based on their  $z_p$  within 500 kpc from the X-ray emission peak

from the initial cluster sample, the distribution is less affected by identifying incorrectly associated BCGs. The median offset of the BCG for the cluster sample is 33 kpc. We investigated a possible evolution of the BCG offset with the cluster redshift. The cluster sample was divided into three subsamples with redshift bins of  $0.05 \leq z < 0.30$ ,  $0.30 \leq z < 0.55$ , and  $0.55 \leq z < 0.80$  and number of clusters 156, 184, and 43, respectively. The median BCG offsets for the low, intermediate, and distant redshift subsamples were 23 kpc, 42 kpc, and 45, respectively. These numbers indicate a trend of increasing positional offset of the BCG with increasing redshift.

We compared the BCGs properties of the cluster sample (383 systems) with the selection criteria of the spectroscopically targeted LRGs in BOSS survey, see Appendix A. We found that 92 percent of the BCGs fulfil the colour and magnitude cuts of the LRGs in BOSS. This high percentage is affected by our strategy

of the cluster identification, which selected a cluster galaxy as an LRG within 200 kpc from the X-ray emission peak.

### 3.4. Comparison with published redshifts

The largest optically selected galaxy cluster sample so far was compiled by Wen et al. (2012, WHL12 hereafter), based on overdensities of galaxies in photometric redshift space from the SDSS-DR8 data. It comprises 132684 clusters with photometric redshift measurements in the range of  $0.05 \leq z < 0.8$ . The catalogue also provides spectroscopic redshifts for about 30 percent of the BCGs. Cross-matching our sample with the WHL12 catalogue yielded 188 common clusters, of these, 131 systems have spectra for the BCGs in their catalogue. We also queried the NASA Extragalactic Database (NED) for available redshift measurements for the remainder of the cluster sample. As a result, 76 clusters with redshift estimates from different projects were found. In total, 264 clusters are previously known in the literature mostly as optically selected galaxy clusters.

Figure 9 shows the comparison between the present redshift measurements and the WHL12 ones as well as the available redshifts from the NED. The good agreement between the current redshift measurements and the published values is clear. The differences between the two measurements,  $\Delta z = z_{\text{present}} - z_{\text{published}}$ , have a mean and standard deviation of 0.0009 and 0.0170, respectively.

We also compared the current redshift measurements with the published ones of the optically confirmed cluster sample from our ongoing survey (Paper II). There are 316 clusters in common between the two samples, of these, 238 have spectroscopic redshifts for at least one cluster galaxy in Paper II. The current procedure spectroscopically confirmed the remainder of the common sample with only photometric redshifts (78 systems). We noted that the current procedure did not identify the whole sample in Paper II with spectroscopic confirmations (310 clusters). This is because we used the criterion of having an LRG with  $z_s$  within 200 kpc. In addition, in Paper II we used the spectroscopic data from the SDSSI/II projects, which provides a galaxy sample with  $z_s$  including LRGs as well as a magnitude-limited galaxy sample that are not necessarily LRGs.

Figure 10 shows the comparison of the present redshift measurements with the values from Paper II of the common sam-

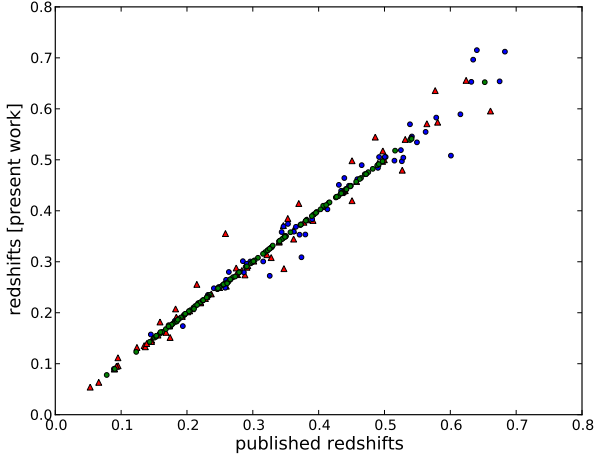


**Fig. 9.** Comparison of the present spectroscopic redshift measurements with the published BCG spectroscopic (green dots) and cluster photometric (blue dots) redshifts by Wen et al. (2012) and the available (either spectroscopic or photometric) redshifts from the NED (red triangle).

ple. The two measurements agree well. The mean and standard deviation of the differences between the measured values,  $\Delta z = z_{\text{present}} - z_{\text{Paper II}}$ , are 0.0039 and 0.0150, respectively. Only 4 percent of the common sample have redshift differences of  $2\sigma < |\Delta z| \leq 4\sigma$ , where  $\sigma = 0.02$  is the uncertainty of the measured photometric redshifts in Paper II. Systems with such redshift differences had only photometric redshifts in our previous work.

We also noted that the present spectroscopic redshifts are not identical with the spectroscopic redshifts in Paper II for a few cases. There are eleven clusters with redshift differences of  $0.01 < |\Delta z| < 0.04$ . This is because cluster galaxies in Paper II were selected within a redshift interval of  $z_{p,\text{BCG}} \pm 0.04(1 + z_{p,\text{BCG}})$ , then the cluster spectroscopic redshift was measured as the weighted average of the available spectroscopic redshifts of these identified cluster galaxies. This led to selecting galaxies with available  $z_s$  that have redshifts outside the redshift interval we used in this work ( $z_{s,\text{BCG}} \pm 0.01$ , see subsection 3.2).

### 3.5. Combined optically confirmed cluster sample from the 2XMMi/SDSS cluster survey

Based on the photometric redshifts of galaxies in the SDSS-DR8, we have optically identified the counterparts of 530 galaxy groups/clusters in Paper II including the cluster sample in Paper I. In the present work, we constructed a cluster sample of 383 systems based on the spectroscopic redshifts of galaxies in the SDSS-DR10. The spectroscopically confirmed cluster sample extends the optically confirmed cluster sample in Paper II by 67 objects. Therefore, out of 1180 X-ray cluster candidates we optically confirmed 597 galaxy groups/clusters (51 percent) and measured their redshifts.

This is the largest X-ray selected galaxy cluster catalogue so far based on the archival XMM-Newton observations. The XMM-Newton sensitivity and the available deep XMM-Newton fields allowed us to detect clusters down to X-ray flux of  $\sim 10^{-15}$  erg cm $^{-2}$  s $^{-1}$  in [0.5 - 2.0] keV. However, this is not a flux-limited cluster sample since we included XMM-Newton observations with different exposure times in our survey. The redshifts

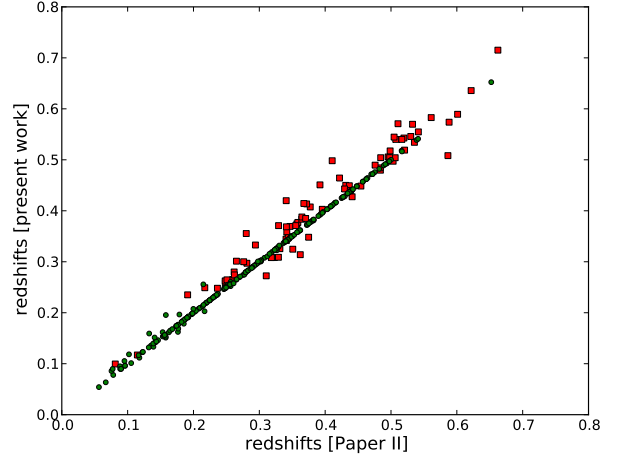


**Fig. 10.** Comparison of the present spectroscopic redshift measurements with the measured spectroscopic redshifts (green dots) and photometric ones (red squares) from Paper II.

of the full cluster sample span a wide range from 0.03 to 0.79 with a median of 0.34. Concerning spectroscopic redshifts, out of 597 confirmed clusters 455 systems (76 percent) have a spectroscopic confirmation based on at least one member galaxy with a spectrum.

Overall, we are left with 583 unconfirmed X-ray cluster candidates (49 percent). These remaining candidates are either distant clusters beyond the SDSS detection limit, systems with low richness that are groups with few members, or possibly spurious detections.

## 4. X-ray parameters

In Paper II, we provided two subsamples of clusters: (i) a cluster subsample comprising 345 objects with their X-ray spectroscopic temperature and flux from the spectral fitting, and (ii) a cluster subsample consisting of 185 systems with their X-ray flux obtained from the 2XMMi-DR3 catalogue, because their X-ray data are insufficient for spectral fitting. For both subsamples, we also estimated the X-ray bolometric luminosity  $L_{500}$  using an iterative method based on scaling relations. This iterative procedure was the same for the two subsamples but with different inputs, see Section 4 in Paper II for more detail about this procedure. We found a good agreement between the derived  $L_{500}$  for the clusters in common between the two subsamples.

In the current work, we estimate the X-ray parameters ( $L_{500}$  and  $M_{500}$ ) for the present optically validated cluster sample (383 systems) based on the integrated  $\beta$  model fluxes that were given in the 2XMMi-DR3 catalogue. Firstly, we compute the X-ray luminosities using the catalogue fluxes and the measured redshifts. Secondly, we convert the computed luminosity to bolometric luminosities  $L_{500}$ . Finally, the estimated  $L_{500}$  are used to compute the cluster masses  $M_{500}$ .

### 4.1. X-ray luminosity and mass

For each system in the current cluster sample, we obtained its X-ray aperture-corrected,  $\beta$ -model, flux that was calculated by the SAS tasks `emldetect` from the 2XMMi-DR3 catalogue (Watson et al. 2009). Here we used the combined EPIC (MOS1, MOS2, PN) flux in (0.5-2.0 keV),  $F_{\text{cat},0.5-2}$ , and its propagated

error. Then we computed the X-ray luminosity in (0.5-2.0 keV),  $L_{\text{cat},0.5-2}$ .

To convert  $L_{\text{cat},0.5-2}$  into bolometric luminosity  $L_{500}$ , we used the properties of the cluster sample with reliable X-ray spectroscopic parameters in Paper II. Among the current optically validated cluster sample, there are 218 clusters with X-ray spectroscopic parameters from the spectral fitting were already published in Paper II. We compared bolometric  $L_{500}$  from Paper II and  $L_{\text{cat},0.5-2}$  from the current procedure of these common systems, as shown in Fig. 11. It shows a linear relation between the two luminosity measurements with a few outliers (about 4 percent), which are contaminated by point sources. The best-fit linear relation after excluding these outliers derived using the BCES orthogonal regression method (Akritas & Bershady 1996) is represented by the solid line in Fig. 11 and is given by

$$\log(L_{500}) = (0.51 \pm 0.02) + (0.91 \pm 0.02) \log(L_{\text{cat},0.5-2}). \quad (1)$$

The error in  $L_{500}$  was calculated by including the error measurement of  $L_{\text{cat},0.5-2}$ , the intrinsic scatter in this relation (Eq. 1), and the propagated errors caused by the uncertainty in the slope and the intercept. The intrinsic scatter value of the relation (Eq. 1) is  $0.15 \pm 0.01$ , which was estimated following the method used by Pratt et al. (2009).

Eq. 1 provides a quick method to derive bolometric  $L_{500}$  based on the measured  $L_{\text{cat},0.5-2}$ . This scaling relation implicitly includes the bolometric correction (with scatter introduced by the X-ray temperature and luminosity in the energy band [0.5-2.0] keV) as well as aperture flux extrapolation to  $R_{500}$  (with scatter introduced by different surface brightness profile parameters).

The estimated bolometric  $L_{500}$  was used to compute the X-ray luminosity-based mass using the  $L_{500} - M_{500}$  relation published by Pratt et al. (2009) of the form

$$M_{500} = 2 \times 10^{14} M_{\odot} \left( \frac{h(z)^{-7/3} L_{500}}{1.38 \times 10^{44} \text{ erg s}^{-1}} \right)^{1/2.08}, \quad (2)$$

where  $h(z)$  is the Hubble constant normalised to its present-day value,  $h(z) = \sqrt{\Omega_M(1+z)^3 + \Omega_\Lambda}$ . We calculated the error in  $M_{500}$  that has contribution from the error in  $L_{500}$ , the intrinsic scatter in Eq. 2, and the propagated errors for the uncertainty in relation's slope and intercept. Finally,  $M_{500}$  was used to compute  $R_{500}$  as

$$R_{500} = \sqrt[3]{3M_{500}/4\pi 500\rho_c(z)}, \quad (3)$$

where  $\rho_c(z)$  is the critical density,  $\rho_c(z) = h(z)^2 3H_0^2/8\pi G$ .

For the whole current cluster sample (383 systems), we derived  $L_{\text{cat},0.5-2}$ ,  $R_{500}$ ,  $L_{500}$  and  $M_{500}$ , as described above. Among this sample, there are 316 clusters in common with the whole sample (530 objects) in Paper II. The current sample extended the optically confirmed cluster sample from our survey by 67 objects and added several clusters at higher redshift up to  $z = 0.79$ . Since we provided the measurements of  $L_{500}$  and  $M_{500}$  for the common sample in Paper II, we only present the catalogue of the extended cluster sample (67 systems) listing their optical and X-ray parameters. In addition to this new sample, we also provide the spectroscopic redshifts and the X-ray properties for 78 clusters among the common sample in Paper II that previously had only photometric redshifts. These two subsamples are compiled in Table 1 with a note referring to each subsample.

Table 1, available in full form at the CDS, lists the new cluster sample (67 objects) from the current work in addition to a subsample (78 systems) that has only photometric redshifts in

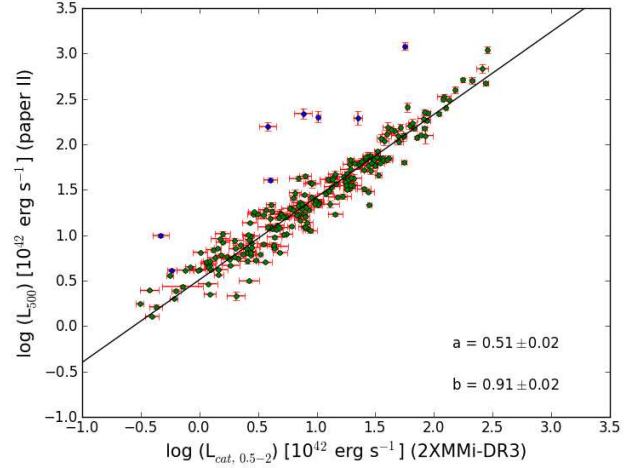


**Fig. 11.** X-ray bolometric luminosity  $L_{500}$  from Paper II plotted against the present luminosity  $L_{\text{cat},0.5-2}$  of 218 clusters in common between the current cluster sample and the sample in Paper II with reliable X-ray parameters. The solid line represents the best fit derived using the BCES orthogonal regression method after excluding eight outliers that are represented by blue dots. The intercept (a) and the slope (b) of the linear relation are written in the lower left corner.

Paper II. The X-ray parameters are estimated based on the flux given in the 2XMMi-DR3 catalogue. Cols. [1] and [2] report the cluster identification number (detection Id, detid) and its name (IAUNAME), cols. [3] and [4] provide the coordinates of X-ray emission in equinox J2000.0. The remaining columns are col. [5] the XMM-Newton observation Id (obsid), col. [6] the cluster spectroscopic redshift, col. [7] the scale at the cluster redshift in kpc'', col. [8] the  $R_{500}$  in kpc, cols. [9] and [10] the 2XMMi-DR3 X-ray flux  $F_{\text{cat}}$  [0.5-2.0] keV and its error in units of  $10^{-14} \text{ erg cm}^{-2} \text{ s}^{-1}$ , cols. [11] and [12] the estimated X-ray luminosity  $L_{\text{cat}}$  [0.5-2.0] keV and its error in units of  $10^{42} \text{ erg s}^{-1}$ , cols. [13] and [14] the cluster bolometric luminosity  $L_{500}$  and its error in units of  $10^{42} \text{ erg s}^{-1}$ , cols. [15] and [16] the cluster mass  $M_{500}$  and its error in units of  $10^{13} M_{\odot}$ , col. [17] the objid of the probable BCG in SDSS-DR10, cols. [18] and [19] the BCG coordinates in equinox J2000.0, col. [20] the apparent model magnitude  $m_r$  of the BCG, col. [21] and [22] the weighted average spectroscopic redshift  $\bar{z}_s$  and the number of cluster members  $N_{z_s}$  within 500 kpc with available spectroscopic redshifts that were used to compute the average redshift, col. [23] and [24] the weighted average photometric redshift  $\bar{z}_p$  and the number of identified cluster member candidates  $N_{z_p}$  within 500 kpc based on their photometric redshifts, col. [25] the projected separation between the cluster X-ray position and the BCG position, cols. [26] the NED name of previously known clusters in the literature, and col. [27] a note indicating the object status, ‘‘Paper III’’ refers to a new system confirmed using the current procedure, and ‘‘Paper II’’ refers to a previously published system in Paper II with only photometric redshift and it is spectroscopically confirmed in the current work.

#### 4.2. Comparison of the derived X-ray parameters

Among the clusters (316 systems) in common between the current cluster sample and that in Paper II, there were 98 clusters published in Paper II with their X-ray properties based on the

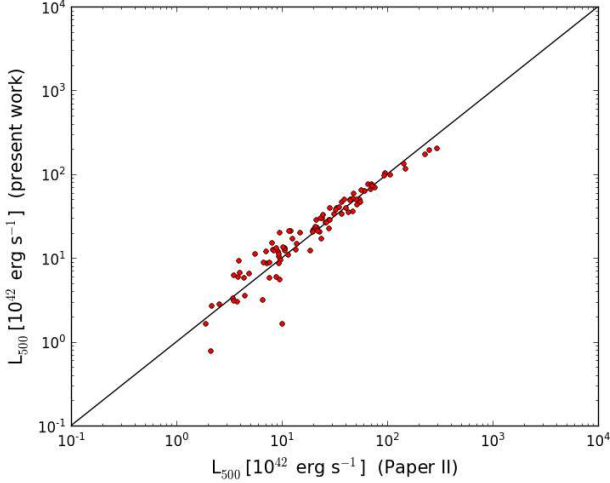
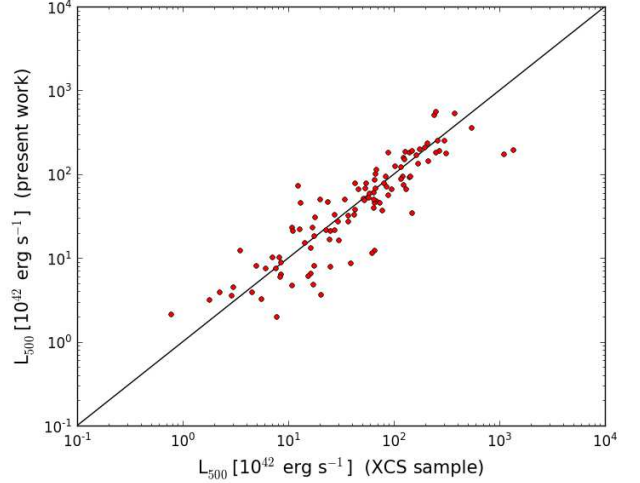


**Fig. 12.** Present measurements of  $L_{500}$  plotted against the corresponding values from Paper II for 98 common clusters with fluxes obtained from the 2XMMi-DR3 catalogue. The solid line represents the one-to-one relationship.

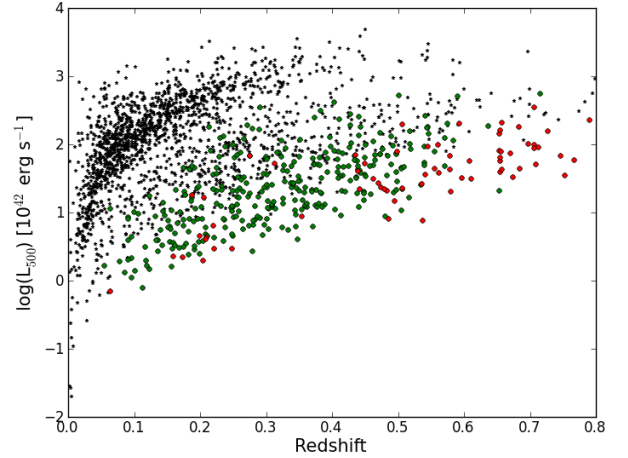
flux given in the 2XMMi-DR3 catalogue. Since we here used a different method to determine the X-ray bolometric  $L_{500}$  from that used in Paper II, we present a comparison of the derived luminosities from the two methods. As shown in Fig. 12, both methods give consistent values of  $L_{500}$ . The only two outliers are at the lowest redshifts (0.05 and 0.11) of the common sample. The median value of the ratios between the present  $L_{500}$  estimates and the values from Paper II is 1.1. This offset of the current estimates of  $L_{500}$  (10 percent) might arise from using two different procedures, the slight difference in the measured redshifts of the common systems, in addition to the two outliers mentioned above.

Figure 13 shows the good agreement between the current  $L_{500}$  estimates and the corresponding values from the XCS project for 107 common objects. The ratio between the present  $L_{500}$  to the corresponding values in the XCS project has a median of 0.95. Of the common sample, 33/107 have only photometric redshifts in the XCS sample, therefore our cluster sample provides spectroscopic confirmation for these systems. In general, there is consistency between the redshift measurements of the common sample apart from ten systems with  $|z_{\text{present}} - z_{\text{XCS}}| > 0.05$ , which have only photometric redshifts in the XCS sample. The mean and standard deviation of the redshift differences ( $z_{\text{present}} - z_{\text{XCS}}$ ) are 0.01 and 0.03, respectively.

The mass range of the cluster sample is  $M_{500} \sim 2 - 28 \times 10^{13} M_{\odot}$  and the bolometric luminosity range is  $L_{500} \sim 1 - 600 \times 10^{42} \text{ erg s}^{-1}$ . Figure 14 shows the distributions of  $L_{500}$  as a function of redshift for the new cluster sample (67 systems) and the objects in common with Paper II (316 objects) as well as for 1730 clusters ( $z < 0.8$ ) from the MCXC catalogue, which was compiled from published X-ray selected cluster catalogues from ROSAT data (Piffaretti et al. 2011). Owing to the sensitivity of XMM-Newton and deeper exposures for some fields, the current cluster sample mostly includes low-luminosity groups and clusters at each redshift, as shown in Fig. 14. Cross-matching our cluster sample with the MCXC catalogue within a radius of 30 arcsec yielded 17 clusters. The current estimates of  $M_{500}$  agree well with the corresponding values in the MCXC catalogue of the common systems, as shown in Fig. 15. The small overlap between the two samples is caused by the relatively small survey



**Fig. 13.** Comparison of the present estimates of  $L_{500}$  and the values from the XCS project for 107 clusters in common. The solid line shows the one-to-one relationship.



**Fig. 14.** Distribution of the X-ray bolometric luminosities,  $L_{500}$ , with redshift of the new cluster sample (red dots) from the current procedure, the cluster sample in common with Paper II (green dots), and a sample of 1730 clusters (black stars) below redshift 0.8 detected from ROSAT data (Piffaretti et al. 2011).

area in our project and by constraining our survey to include only systems identified as serendipitously detected sources and not targets in XMM-Newton observations.

In the new sample that comprises 67 X-ray selected clusters, only 12 systems were previously known as X-ray detected clusters. They were published by Mehrrens et al. (2012), Clerc et al. (2012), Piffaretti et al. (2011), or Finoguenov et al. (2007). In total, about 25 percent of this new sample were previously known either in optical or X-ray band, the remainder of this sample are new systems.

In Paper II, we presented the  $L_X - T$  relation based on a cluster sample comprising 345 systems in the redshift range  $0.03 < z < 0.67$ . In the future, we plan to extend the  $L_X - T$  relation to include distant clusters up to slightly higher redshifts from the newly constructed cluster sample in this work. Since the current cluster sample provides spectroscopic confirmation for 78 clusters of the cluster sample published in paper II, we

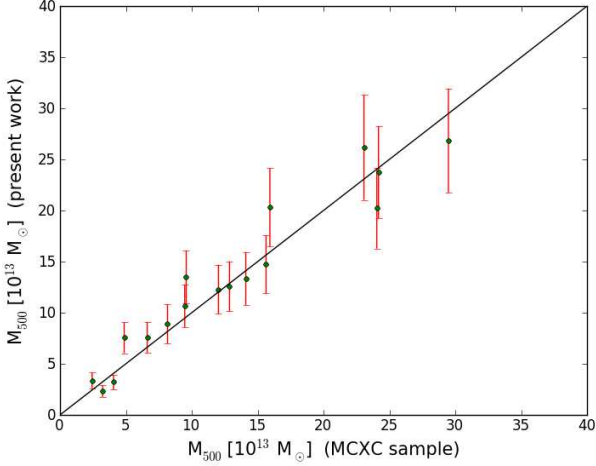


**Fig. 15.** Measurements of  $M_{500}$  from our survey plotted against values from the MCXC catalogue for 17 clusters in common with ours. The solid line shows the one-to-one relationship.

can re-measure their X-ray parameters with a better accuracy, which might help in reducing the scatter in the  $L_X - T$  relation. We also plan to investigate the correlations between the X-ray and optical properties of the full cluster sample from our cluster survey that are optically confirmed so far.

## 5. Summary

We presented a sample of 383 X-ray selected galaxy groups and clusters associated with at least one LRG, which has a spectroscopic redshift in the SDSS-DR10. The redshifts of the associated LRGs were used to identify BCGs and other cluster galaxies with spectroscopic redshifts. The cluster spectroscopic redshift was computed as the weighted average of the available spectroscopic redshifts of the cluster galaxies within 500 kpc from the X-ray emission peak. The cluster sample spans a wide redshift range of  $0.05 \leq z \leq 0.79$  with a median of  $z = 0.34$ . Of the cluster sample, 264 are previously known as optically selected galaxy clusters. In addition to re-identifying and confirming the redshift estimates of 316 clusters in common with the published cluster sample from our survey, we extended the optically confirmed cluster sample by 67 objects. Of this new sample that comprises 67 systems, about 75 percent are newly discovered groups and clusters, and about 80 percent are new X-ray detected clusters. Comparing the BCGs of the cluster sample with the colour and magnitude cuts of LRGs in the BOSS survey yielded that 92 percent of the BCGs are considered LRGs. However, this percentage is dependent on the selection of the spectroscopically targeted LRGs in SDSS as well as on the current cluster identification procedure.

The measured redshift and the X-ray flux in 0.5-2.0 keV given in the 2XMMi-DR3 catalogue were used to determine the X-ray luminosity in 0.5-2.0 keV of the cluster sample. We converted the X-ray luminosity in 0.5-2.0 keV into bolometric luminosity  $L_{500}$  based on the available properties of the published cluster sample with X-ray spectroscopic parameters from our survey. This conversion yielded a scaling relation, which could be used to derive bolometric  $L_{500}$  from the luminosity (0.5-2.0 keV) that is computed based on the  $\beta$  model flux (0.5-2.0 keV) given in the 2XMMi-DR3 catalogue.

We also derived X-ray-luminosity-based masses of the cluster sample based on published scaling relation in the literature. Comparing the current estimates of the X-ray bolometric luminosity,  $L_{500}$ , with the available values from the XCS project, we found a good agreement between the two measurements. The distribution of X-ray luminosities of our cluster sample and ROSAT clusters with redshifts showed that we detected less-luminous groups and clusters at each redshift interval, and added a few tens of clusters at high redshifts.

*Acknowledgements.* This work is supported by the Egyptian Ministry of Higher Education and Scientific Research (MHESR) in cooperation with the Leibniz-Institut für Astrophysik Potsdam (AIP), Germany. We also acknowledge the financial support from the ARCHES project (7th Framework of the European Union, n° 313146) and the support by the Deutsches Zentrum für Luft- und Raumfahrt (DLR) under contract number 50 QR 0802. This work is based on observations obtained with XMM-Newton, an ESA science mission with instruments and contributions directly funded by ESA Member States and the USA (NASA). This research has made use of the NASA/IPAC Extragalactic Database (NED) which is operated by the Jet Propulsion Laboratory, California Institute of Technology, under contract with the National Aeronautics and Space Administration. Funding for SDSS-III has been provided by the Alfred P. Sloan Foundation, the Participating Institutions, the National Science Foundation, and the U.S. Department of Energy. The SDSS-III web site is <http://www.sdss3.org/>. SDSS-III is managed by the Astrophysical Research Consortium for the Participating Institutions of the SDSS-III Collaboration including the University of Arizona, the Brazilian Participation Group, Brookhaven National Laboratory, University of Cambridge, University of Florida, the French Participation Group, the German Participation Group, the Instituto de Astrofísica de Canarias, the Michigan State/Notre Dame/JINA Participation Group, Johns Hopkins University, Lawrence Berkeley National Laboratory, Max Planck Institute for Astrophysics, New Mexico State University, New York University, Ohio State University, Pennsylvania State University, University of Portsmouth, Princeton University, the Spanish Participation Group, University of Tokyo, University of Utah, Vanderbilt University, University of Virginia, University of Washington, and Yale University.

## Appendix A: Selection criteria of LRGs

We used the colour and magnitude cuts that were used to select spectroscopic targets to construct the BOSS galaxy sample in the the SDSS-III project. The selection criteria of galaxies targeted in BOSS were given in Padmanabhan et al. (2014) and were provided on the BOSS homepage<sup>4</sup>. The BOSS includes two samples of galaxies, one is the BOSS “LOWZ” Galaxy Sample,  $z \leq 0.4$ . The selection cuts are as follows:

1.  $|c_{\perp}| < 0.2$ , to define the colour boundaries of the sample around a passive stellar population, where  $c_{\perp} = (r - i) - (g - r)/4.0 - 0.18$ .
2.  $r < 13.5 + c_{\parallel}/0.3$ , to select the brightest galaxies at each redshift, where  $c_{\parallel} = 0.7(g - r) + 1.2[(r - i) - 0.18]$ .
3.  $16 < r < 19.6$ , to define the faint and bright limits.

The other is the BOSS “CMASS” Galaxy Sample,  $0.4 < z < 0.8$ . The colour and magnitude cuts are as follows:

1.  $d_{\perp} > 0.55$ , to isolate high-redshift objects, where  $d_{\perp} = (r - i) - (g - r)/8.0$ .
2.  $i < 19.86 + 1.6(d_{\perp} - 0.8)$ , to select the brightest or more massive galaxies with redshift.
3.  $17.5 < i < 19.9$ , to define the faint and bright limits.
4.  $r - i < 2$ , to protect from some outliers.

Note that we did not apply the criteria that were used to perform a star-galaxy separation since we only considered objects that were classified as galaxies indicated by spectroscopic class

<sup>4</sup> [http://www.sdss3.org/dr10/algorithms/boss\\_galaxy\\_ts.php](http://www.sdss3.org/dr10/algorithms/boss_galaxy_ts.php)

parameters given in the `SpecObj` table. Note also that all colours were computed using model magnitudes while the magnitude cuts were applied on composite model (`cmodel`) magnitudes. All magnitudes were corrected for Galactic extinction following Schlegel et al. (1998).

Šuhada, R., Song, J., Böhringer, H., et al. 2012, *A&A*, 537, A39  
 Vikhlinin, A., Kravtsov, A. V., Burenin, R. A., et al. 2009, *ApJ*, 692, 1060  
 Voit, G. M. 2005, *Reviews of Modern Physics*, 77, 207  
 Watson, M. G., Schröder, A. C., Fyfe, D., et al. 2009, *A&A*, 493, 339  
 Wen, Z. L., Han, J. L., & Liu, F. S. 2009, *ApJS*, 183, 197  
 Wen, Z. L., Han, J. L., & Liu, F. S. 2012, *ApJS*, 199, 34  
 Zwicky, F., Herzog, E., & Wild, P. 1961, Pasadena: California Institute of Technology, volume I

## References

- Abell, G. O. 1958, *ApJS*, 3, 211  
 Abell, G. O., Corwin, Jr., H. G., & Olowin, R. P. 1989, *ApJS*, 70, 1  
 Adami, C., Mazure, A., Pierre, M., et al. 2011, *A&A*, 526, A18  
 Ahn, C. P., Alexandroff, R., Allende Prieto, C., et al. 2013, *ArXiv e-prints*  
 Ahn, C. P., Alexandroff, R., Allende Prieto, C., et al. 2012, *ApJS*, 203, 21  
 Akritas, M. G. & Bershady, M. A. 1996, *ApJ*, 470, 706  
 Allen, S. W., Evrard, A. E., & Mantz, A. B. 2011, *ARA&A*, 49, 409  
 Anderson, M. E., Bregman, J. N., Butler, S. C., & Mullis, C. R. 2009, *ApJ*, 698, 317  
 Bahcall, N. A. 1988, *ARA&A*, 26, 631  
 Balestra, I., Tozzi, P., Ettori, S., et al. 2007, *A&A*, 462, 429  
 Barkhouse, W. A., Green, P. J., Vikhlinin, A., et al. 2006, *ApJ*, 645, 955  
 Bartelmann, M. 2010, *Classical and Quantum Gravity*, 27, 233001  
 Böhringer, H. 2006, *X-ray Studies of Clusters of Galaxies, The Universe in X-rays*  
 Böhringer, H., Schuecker, P., Guzzo, L., et al. 2004, *A&A*, 425, 367  
 Burenin, R. A., Vikhlinin, A., Hornstrup, A., et al. 2007, *ApJS*, 172, 561  
 Clerc, N., Sadibekova, T., Pierre, M., et al. 2012, *MNRAS*, 3120  
 Cora, S. A. 2006, *MNRAS*, 368, 1540  
 de Hoon, A., Lamer, G., Schwobe, A., et al. 2013, *A&A*, 551, A8  
 Dressler, A. 1980, *ApJ*, 236, 351  
 Durret, F., Adami, C., Cappi, A., et al. 2011, *A&A*, 535, A65  
 Ebeling, H., Edge, A. C., Böhringer, H., et al. 1998, *MNRAS*, 301, 881  
 Ebeling, H., Edge, A. C., Mantz, A., et al. 2010, *MNRAS*, 407, 83  
 Eisenstein, D. J., Annis, J., Gunn, J. E., et al. 2001, *AJ*, 122, 2267  
 Fassbender, R., Böhringer, H., Nastasi, A., et al. 2011, *New Journal of Physics*, 13, 125014  
 Finoguenov, A., Guzzo, L., Hasinger, G., et al. 2007, *ApJS*, 172, 182  
 Finoguenov, A., Watson, M. G., Tanaka, M., et al. 2010, *MNRAS*, 403, 2063  
 Geach, J. E., Murphy, D. N. A., & Bower, R. G. 2011, *MNRAS*, 413, 3059  
 Gettings, D. P., Gonzalez, A. H., Stanford, S. A., et al. 2012, *ApJ*, 759, L23  
 Gladders, M. D. & Yee, H. K. C. 2005, *ApJS*, 157, 1  
 Goto, T., Sekiguchi, M., Nichol, R. C., et al. 2002, *AJ*, 123, 1807  
 Goto, T., Yamauchi, C., Fujita, Y., et al. 2003, *MNRAS*, 346, 601  
 Hao, J., McKay, T. A., Koester, B. P., et al. 2010, *ApJS*, 191, 254  
 Hasselfield, M., Hilton, M., Marriage, T. A., et al. 2013, *J. Cosmology Astropart. Phys.*, 7, 8  
 Heath, D., Krause, M., & Alexander, P. 2007, *MNRAS*, 374, 787  
 Koester, B. P., McKay, T. A., Annis, J., et al. 2007, *ApJ*, 660, 239  
 Kolokotronis, V., Georgakakis, A., Basilakos, S., et al. 2006, *MNRAS*, 366, 163  
 Lamer, G., Hoefl, M., Kohnert, J., Schwobe, A., & Storm, J. 2008, *A&A*, 487, L33  
 Maughan, B. J., Jones, C., Forman, W., & Van Speybroeck, L. 2008, *ApJS*, 174, 117  
 Mehrrens, N., Romer, A. K., Hilton, M., et al. 2012, *MNRAS*, 2912  
 Merchán, M. E. & Zandivarez, A. 2005, *ApJ*, 630, 759  
 Metcalfe, L., Kneib, J.-P., McBreen, B., et al. 2003, *A&A*, 407, 791  
 Ota, N. 2012, *Research in Astronomy and Astrophysics*, 12, 973  
 Piffaretti, R., Arnaud, M., Pratt, G. W., Pointecouteau, E., & Melin, J.-B. 2011, *A&A*, 534, A109  
 Planck Collaboration, Ade, P. A. R., Aghanim, N., et al. 2013, *ArXiv e-prints*  
 Postman, M. & Lauer, T. R. 1995, *ApJ*, 440, 28  
 Pratt, G. W., Croston, J. H., Arnaud, M., & Böhringer, H. 2009, *A&A*, 498, 361  
 Reichardt, C. L., Stalder, B., Bleem, L. E., et al. 2013, *ApJ*, 763, 127  
 Reiprich, T. H. & Böhringer, H. 2002, *ApJ*, 567, 716  
 Rosati, P., Borgani, S., & Norman, C. 2002, *ARA&A*, 40, 539  
 Rosati, P., della Ceca, R., Norman, C., & Giacconi, R. 1998, *ApJ*, 492, L21  
 Rykoff, E. S., McKay, T. A., Becker, M. R., et al. 2008, *ApJ*, 675, 1106  
 Rykoff, E. S., Rozo, E., Busha, M. T., et al. 2013, *ArXiv e-prints*  
 Santos, M. R., Ellis, R. S., Kneib, J.-P., Richard, J., & Kuijken, K. 2004, *ApJ*, 606, 683  
 Sarazin, C. L. 1988, *X-ray emission from clusters of galaxies* (Cambridge, UK: Cambridge Univ. Press)  
 Schlegel, D. J., Finkbeiner, D. P., & Davis, M. 1998, *ApJ*, 500, 525  
 Szabo, T., Pierpaoli, E., Dong, F., Pipino, A., & Gunn, J. 2011, *ApJ*, 736, 21  
 Takey, A., Schwobe, A., & Lamer, G. 2011, *A&A*, 534, A120  
 Takey, A., Schwobe, A., & Lamer, G. 2013, *A&A*, 558, A75  
 Tundo, E., Moretti, A., Tozzi, P., et al. 2012, *A&A*, 547, A57

**Table 1.** The first ten entries of the new cluster sample (67 objects) from the current work in addition to a subsample (78 systems) that has only photometric redshifts in common with Paper II. The X-ray parameters are determined based on the flux given in the 2XMMi-DR3 catalogue.

detid <sup>a</sup>	Name <sup>a</sup> IAUNAME	ra <sup>a</sup> (deg)	dec <sup>a</sup> (deg)	obsid <sup>a</sup>	z <sup>b</sup>	scale kpc''	R <sub>500</sub> (kpc)	F <sub>cat</sub> <sup>a,c</sup>	±eF <sub>cat</sub>	L <sub>cat</sub> <sup>d</sup>	±eL <sub>cat</sub>	L <sub>500</sub> <sup>e</sup>	±eL <sub>500</sub>	M <sub>500</sub> <sup>f</sup>	±eM <sub>500</sub>
(1)	(2)	(3)	(4)	(5)	(6)	(7)	(8)	(9)	(10)	(11)	(12)	(13)	(14)	(15)	(16)
005735	2XMM J003840.4+004746	9.66841	0.79636	0203690101	0.5553	6.44	542.28	1.44	0.18	17.86	2.20	44.88	5.02	8.31	1.69
007554	2XMM J004304.2-092801	10.76751	-9.46695	0065140201	0.1866	3.12	585.47	6.84	1.06	6.74	1.05	18.50	2.61	6.87	1.45
010986	2XMM J005556.9+003806	13.98720	0.63507	0303110401	0.2047	3.36	570.81	5.01	0.95	6.06	1.15	16.81	2.91	6.49	1.41
016221	2XMM J012341.3+072323	20.92215	7.38985	0300000301	0.3418	4.86	640.75	5.90	0.85	23.02	3.33	56.53	7.43	10.68	2.17
021043	2XMM J015558.5+053159	28.99394	5.53329	0153030701	0.4499	5.76	658.59	5.82	0.85	43.43	6.37	100.68	13.43	13.14	2.64
021597	2XMM J020019.2+001931	30.08012	0.32553	0101640201	0.6825	7.07	629.03	4.17	0.52	85.10	10.59	185.57	20.98	15.09	2.98
030746	2XMM J023346.9-085054	38.44543	-8.84844	0150470601	0.2653	4.08	615.99	5.95	1.09	12.93	2.36	33.47	5.55	8.71	1.84
030889	2XMM J023458.7-085055	38.74463	-8.84868	0150470601	0.2590	4.01	581.98	4.15	0.53	8.54	1.09	22.96	2.67	7.29	1.51
089821	2XMM J083114.4+523447	127.81014	52.57993	0092800201	0.6107	6.74	495.95	0.79	0.11	12.25	1.64	31.86	3.88	6.79	1.42
089885	2XMM J083146.1+525056	127.94516	52.84719	0092800201	0.5190	6.23	616.14	3.50	0.21	36.78	2.24	86.56	4.80	11.67	2.26

**Table 1.** continued.

detid <sup>a</sup>	objid <sup>g</sup> (BCG)	RA <sup>g</sup> (deg)	DEC <sup>g</sup> (deg)	m <sub>r</sub> <sup>g</sup> (BCG)	z <sub>s</sub> <sup>g</sup>	N <sub>z<sub>s</sub></sub> <sup>g</sup>	z <sub>p</sub> <sup>g</sup>	N <sub>z<sub>p</sub></sub> <sup>g</sup>	offset <sup>g</sup> (kpc)	NED-Name	note <sup>h</sup>
(1)	(17)	(18)	(19)	(20)	(21)	(22)	(23)	(24)	(25)	(26)	(27)
005735	1237663204918428144	9.68054	0.78241	20.047	0.5553	3	0.5127	7	429.63	-	Paper-III
007554	1237652630713860232	10.80832	-9.47863	17.213	0.1866	2	0.1794	18	473.45	-	Paper-III
010986	1237663784740388918	14.02537	0.62659	17.537	0.2047	3	0.1951	20	473.61	-	Paper-III
016221	1237669767089357103	20.92160	7.39115	18.557	0.3418	1	0.3327	14	24.64	-	Paper-II
021043	1237678663047250389	28.98754	5.53072	19.553	0.4499	1	0.4258	12	142.32	-	Paper-II
021597	1237657071160263439	30.08100	0.32491	20.448	0.6825	1	0.6555	3	27.36	SEXCLAS 03	Paper-III
030746	1237653500970139807	38.44673	-8.84925	17.540	0.2653	1	0.2547	17	22.30	WHL J023347.2-085057	Paper-II
030889	1237653500970270877	38.74547	-8.84926	17.762	0.2590	2	0.2528	17	14.70	-	Paper-II
089821	1237651701914141241	127.80965	52.57912	20.467	0.6107	1	0.6465	4	20.97	-	Paper-III
089885	1237651272960967114	127.94343	52.84937	19.251	0.5190	2	0.5165	13	54.28	WHL J083146.4+525057	Paper-II

**Notes.** The entire cluster catalogue is available online at CDS. <sup>(a)</sup> Parameters extracted from the 2XMMi-DR3 catalogue. <sup>(b)</sup> Spectroscopic redshift as given in col. (21). <sup>(c)</sup> 2XMMi-DR3 flux, F<sub>cat</sub> [0.5-2.0] keV, and its errors in units of 10<sup>-14</sup> erg cm<sup>-2</sup> s<sup>-1</sup>. <sup>(d)</sup> X-ray luminosity, L<sub>cat</sub> [0.5-2.0] keV, and its errors in units of 10<sup>42</sup> erg s<sup>-1</sup>. <sup>(e)</sup> X-ray bolometric luminosity at R<sub>500</sub>, L<sub>500</sub> and its error in units of 10<sup>42</sup> erg s<sup>-1</sup>. <sup>(f)</sup> X-ray-luminosity-based mass at R<sub>500</sub>, M<sub>500</sub> and its error in units of 10<sup>13</sup> M<sub>⊙</sub>. <sup>(g)</sup> Parameters obtained from the current detection algorithm in the optical band. <sup>(h)</sup> A note about each system as “Paper III”: new cluster from the current work and “paper-II”: a cluster in Paper II and confirmed spectroscopically with the present procedure.